Formation of Nematic Liquid Crystals of Sterically Stabilized Layered Double Hydroxide Platelets

Maurice C. D. Mourad,* Edwin J. Devid, Matti M. van Schooneveld, Chantal Vonk, and Henk N. W. Lekkerkerker

van't Hoff Laboratory for Physical and Colloid Chemistry, Utrecht University, P.O. Box 80.051, 3508 TB Utrecht, The Netherlands

Received: April 10, 2008; Revised Manuscript Received: May 21, 2008

Colloidal platelets of hydrotalcite, a layered double hydroxide, have been prepared by coprecipitation at pH 11−12 of magnesium nitrate and aluminum nitrate at two different magnesium to aluminum ratios. Changing the temperature and ionic strength during hydrothermal treatment, the platelets were tailored to different sizes and aspect ratios. Amino-modified polyisobutylene molecules were grafted onto the platelets following a convenient new route involving freeze-drying. Organic dispersions in toluene were prepared of the particles with the largest size and highest aspect ratio. The colloidal dispersions prepared in this way showed isotropic−nematic phase transitions above a limiting concentration in a matter of days. The number density at the transition and the width of the biphasic region were determined and compared to theory. The orientation of the platelets in nematic droplets (tactoids) and at the isotropic−nematic interface were analyzed by polarization microscopy. It was observed that sedimentation induces a nematic layer in samples that are below the limiting concentration for isotropic−nematic phase separation. No nematic phase was observed in the initial aqueous suspensions of the ungrafted particles.

1. Introduction

The isotropic to nematic transition in dispersions of anisotropic mineral colloids has been subject of renewed interest during the last 20 years.[1,2] After the first observations of such a transition for V_2O_5,[3] α-FeOOH,[4] and california bentonite,[5] which nowadays is recognized as hectorite,[6] and the consequent theoretical treatment of the phenomenon by Onsager,[7] there has been a considerable silence in the experimental field. In recent years, however, the so-called mineral liquid crystals have re-emerged and isotropic to nematic transitions have now been observed as well for aqueous boehmite,[8,9] imogolite,[10] akaganeite,[11–13] goethite,[14] gibbsite,[15] layered double hydroxides[16] and nontronite,[17] and sterically stabilized boehmite,[9] gibbsite,[18] and sepiolite.[19]

The layered double hydroxide (LDH) platelets are particularly interesting, since they form an easy-to-synthesize class of colloidal, disk shaped materials that can be adapted chemically to contain different metal ions and intercalated anions. The general formula for LDHs is:

$$\left[M_{1-x}^{2+}M_x^{3+}(\mathrm{OH})_2\right]^{x+}\left[A_{x/y}^{y-}\right]^{x-}\cdot m\mathrm{H_2O}$$

with M^{2+} and M^{3+} being the divalent and trivalent metal cations, respectively. The structure is obtained when part of the divalent cations is substituted by trivalent cations with a similar ionic radius while the brucite-like structure is maintained. The ability of introducing significant amounts of trivalent cations makes the LDH particles have interesting tunable optical and magnetic properties. Hydrotalcite is the LDH that consists of Mg^{2+} and Al^{3+}. This mineral is easy to synthesize, and the preparation is well described.[20–22]

Sun et al. demonstrated the ability of water dispersed hydrotalcite platelets to phase separate into nematic[16] and lamellar[23] structures. Moreover, addition of a depletion agent by means of nonadsorbing polymer led to multiphase equilibria.[24] The interaction between the individual particles in these experiments is dominated by the repulsion of the particles through their charge and, in the latter case, by the depletion attraction. The contribution of the electrostatical double layer to this interaction decreases the effective anisotropy[15] and may result in phase behavior not expected on entropic grounds.[15,25,26] In contrast, polymer grafted particles may be regarded as elements with almost hard interactions for which entropy dominates the phase behavior.

In the work presented here, the synthesis of hydrotalcite is performed by alkaline coprecipitation of metal nitrates.[22] Furthermore, experiments at different temperatures and peptization were performed to control the size.[21] The average particle diameter plays an important role: the presence of an electric double layer or a grafted polymer layer will decrease the aspect ratio (size over thickness: d/l). The larger the size of the platelet, the smaller the effect of these layers on the aspect ratio is. Computer simulations[27] predict that for $(d/l) \leq 7$ the isotropic−nematic transition is no longer thermodynamically stable and is replaced by an isotropic−columnar transition. This is demonstrated in experiments with nickel hydroxide platelets.[28] Moreover, in the case of columnar liquid crystals, a particle diameter that is too small will cause Bragg reflections to occur at wavelengths below the visible range. On the other hand, too large particle sizes have been observed to prevent phase separation in sedimentation experiments.[25]

Using a novel approach, the hydrotalcite particles were grafted with amino-functionalized polyisobutylene (PIB) chains which are known for their successful stabilization of inorganic particles. PIB proved its use in other liquid crystal forming systems.[9,18,19] Dispersions of sterically stabilized hydrotalcite particles in toluene have a very low turbidity due to refractive index matching and are able to phase separate in a few days, compared

* To whom correspondence should be addressed. E-mail: m.c.d.mourad@uu.nl.

10.1021/jp803114v CCC: $40.75
Published on Web 07/24/2008

TABLE 1: Average Diameter and Relative Standard Deviation of the Diameter As Measured by Electron Microscopy on Hydrotalcite Platelets Synthesized at Various Experimental Conditions[a]

system	ratio Mg^{2+}/Al^{3+}	θ (°C)	centrifuged	d (nm)	σ_d
A	2:1	22		46	0.33
B	2:1	85		65	0.27
C	2:1	150	yes	146	0.26
D	4:1	85		51	0.29
E	4:1	85	yes	69	0.35
F	4:1	150	yes	133	0.33

[a] Variables are the mole fraction of Mg^{2+}/Al^{3+} and the insertion of a step in which the precipitate is sedimented by centrifugation and redispersed in Millipore water before hydrothermal treatment.

to months for similar aqueous systems.[16] Earlier, nonaqueous suspensions of liquid crystal forming mineral particles were obtained by an elaborate method which involves a gradual solvent substitution upon addition of the stabilizing polymer.[29,30] Here, we describe an alternative method in which the particles are freeze-dried in the presence of the stabilizer as has been applied before successfully to graft surfactants on cellulose whiskers.[31] The resulting organophilic hydrotalcite particle maybe a usefull starting material in the preparation of polymer colloid nanocomposites.[32]

2. Experimental Section

2.1. Preparation. Colloidal hydrotalcite platelets were synthesized by coprecipitation at pH 11−12. $Mg(NO_3)_2 \cdot 6H_2O$ (Acros Organics, p.a.) and $Al(NO_3)_3 \cdot 9H_2O$ (Aldrich, 98% p.a.), with the total concentration of the Mg and Al ion content equal to 0.5 M, were added dropwise to an equal volume of alkaline solution containing 1.1 M NaOH (Merck, p.a.) and 0.15 M $NaNO_3$ (Merck, p.a.).[22] All water used for the preparation was Millipore (Synergy, Millipore company) or doubly distilled water. Two magnesium to aluminum ratios of the reactants were used to obtain different systems: 2:1 and 4:1.

After coprecipitation, some of the suspensions were hydrothermally treated in their mother liquid, while others were centrifuged (900 g, 40 min) and redispersed in water before. This treatment is expected to improve the growth and crystallinity of the resulting particles.[21] The mixtures were stirred at fixed temperature (of 22, 85, and 150 °C) for 3 days. For each batch, the ratio of the reactants, the temperature during hydrothermal treatment, and the insertion of a redispersion step are presented in Table 1. Finally, the suspensions were dialyzed in tubes (regenerated cellulose, Visking, MWCO 12 000−14 000) against demineralized water until the conductivity dropped below 10 μS/cm and centrifuged in order to concentrate and fractionate (typically at 1000g, 17 h; Beckman Coulter, Avanti J20-XP).

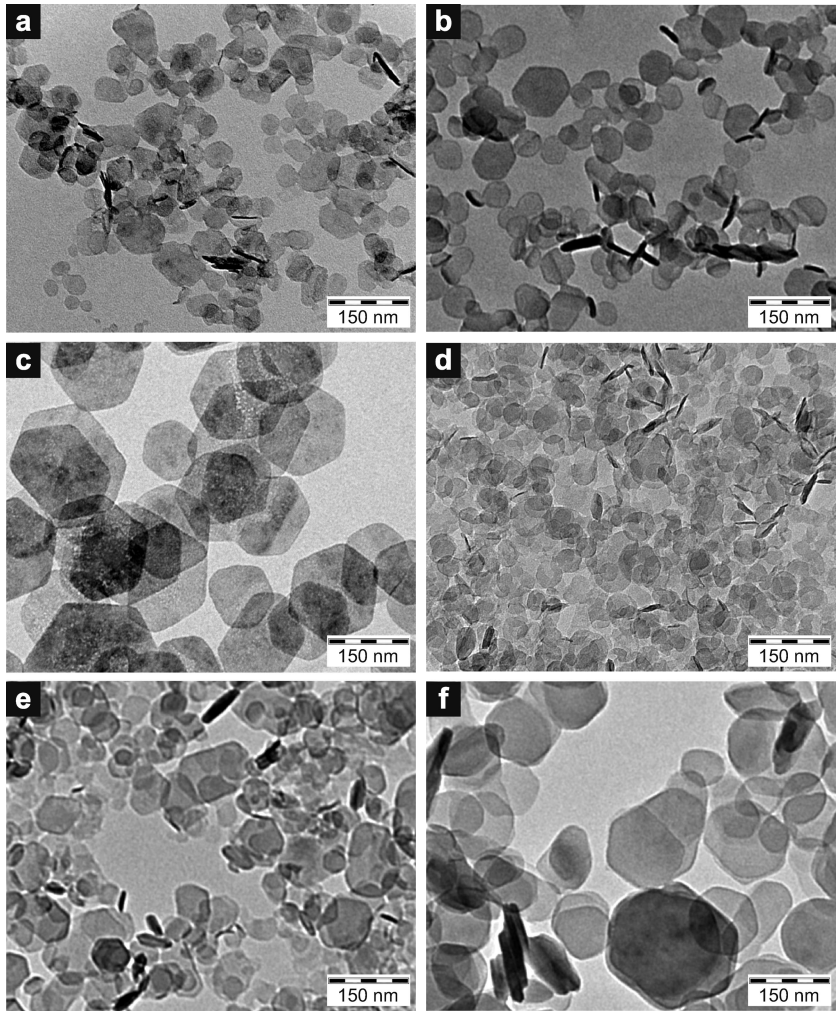

Figure 1. Transmission electron micrographs of the hydrotalcite platelets synthesized. Panels a−f correspond to systems A−F as defined in Table 1. Clearly visible is the hexagonal shape with slightly rounded corners for all systems.

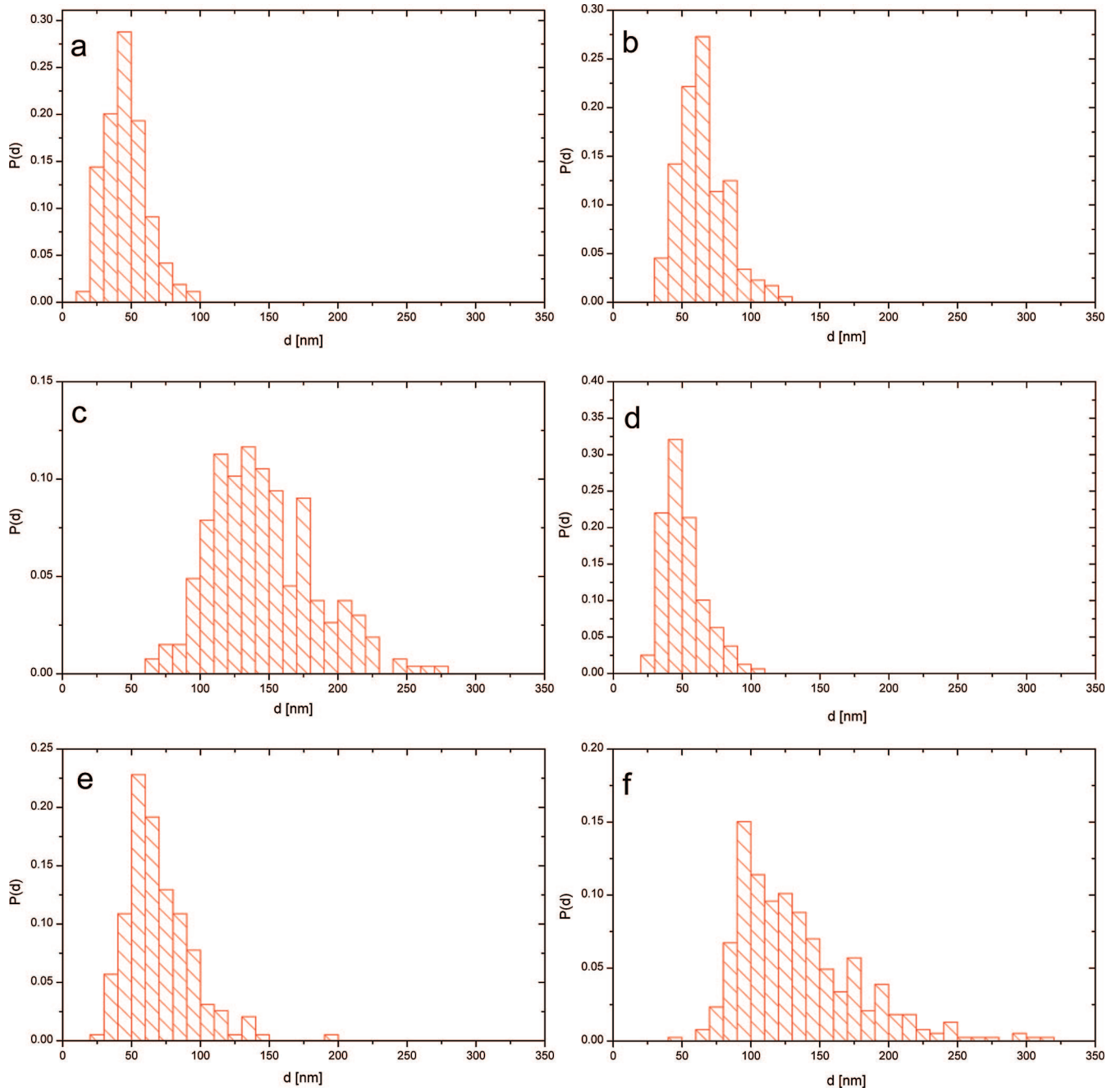

Figure 2. Diameter distributions of hydrotalcite platelets. Transmission electron micrographs were analyzed using the method described in section 2.2. Panels a−f correspond to systems A−F as defined in Table 1.

TABLE 2: Crystallographic Data for Hydrotalcite Systems Obtained via Various Synthetic Routes[a]

system	*a* (Å)	*b* (Å)	*c* (Å)	remarks
C	6.35	6.37	47.92	
D	6.28	6.56	49.40	some contamination
E	6.32	6.43	49.34	some contamination
F	6.31	6.43	49.00	additional bayerite phase present

[a] The crystallographic unit cell was calculated by fitting the diffractograms to the *R*3*m* space group.

The system with the largest hydrotalcite platelets (system C, as indicated in Table 1) was grafted with sterical stabilizer in order to obtain an organophilic system. The polymer used to graft the mineral material is amino-modified polyisobutylene stabilizer SAP 230 TP having two tails of approximately 17 isobutylene subunits. A mixture of 1-propanol (80 mL Acros, 99%) and SAP 230 TP (Infineum, U.K., 10 g) was stirred mechanically until the polymer appeared well dispersed. Aqueous hydrotalcite dispersion (100 mL, 79 g/dm^3) was added dropwise to the mixture. The solvent was then removed by using a rotational vacuum evaporator until a highly viscous paste was obtained. The product was spread out as a film at the inside of a round-bottom flask and was frozen in liquid nitrogen and connected to a vacuum setup. After freeze-drying, a mixture of hydrotalcite particles and stabilizing polymer was obtained, which was easily redispersable in toluene (J.T. Baker, 99.5%). Finally, excess SAP 230TP was removed by three cycles of centrifugation (2 h, 900*g*) and redispersion in toluene. Concentration series of sterically stabilized hydrotalcite dispersions in toluene were made with overall concentrations ranging from 300 to 700 g/dm^3 by centrifugation and redispersion.

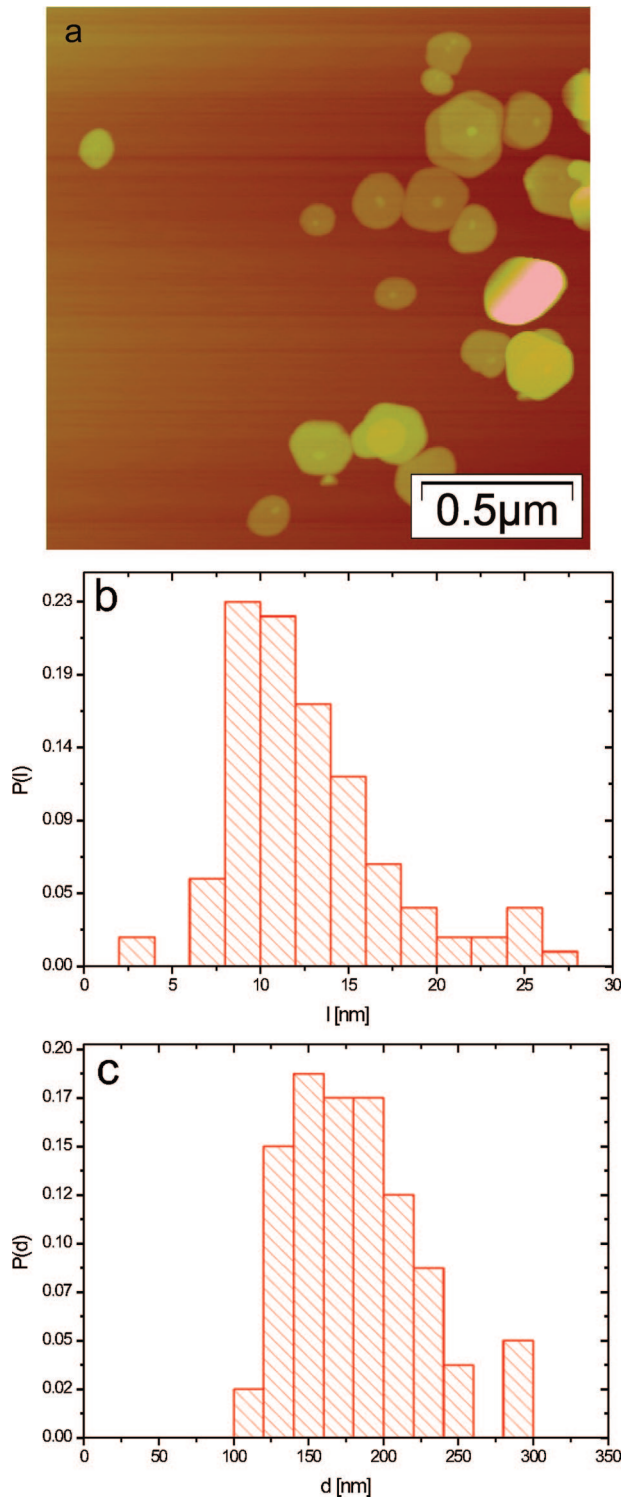

Figure 3. AFM measurements on hydrotalcite platelets. In panel (a), an AFM image of hydrotalcite platelets on a mica support is displayed. In panel (b), a histogram of the thickness of the platelets, as measured by AFM, is shown ($\langle l \rangle = 12.7$ nm with $\sigma_l = 0.36$). In panel (c), the platelet diameter distribution from AFM is depicted ($\langle d \rangle = 182$ with $\sigma_d = 0.23$).

2.2. Particle Characterization. Individual platelets were studied by transmission electron microscopy (TEM) and atomic force microscopy (AFM). For TEM, hydrotalcite particles were dried on polymer films which were sputter coated with carbon for enhanced electrical conductance and supported on copper grids. The electron microscopes (Tecnai 10 and Tecnai 12, FEI Company) were operated at 100 and 120 keV, respectively. The

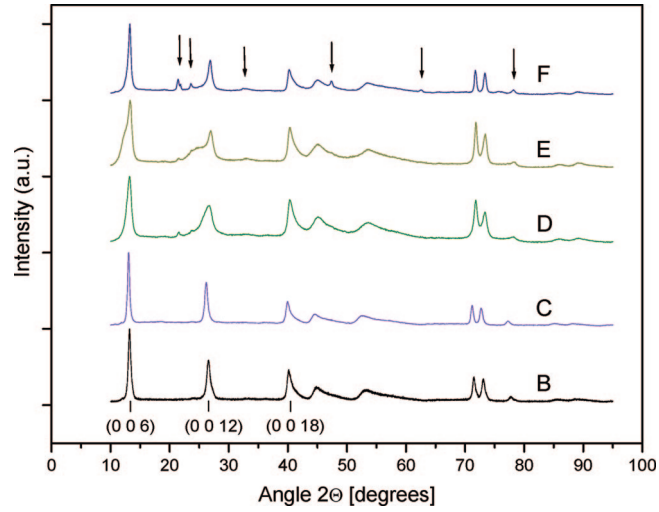

Figure 4. X-ray powder diffractograms of the different hydrotalcites studied (B−F, as defined in Table 1). The baseline of the diffractograms was shifted vertically for clarity. Arrows indicate peaks that are attributed to the presence of a bayerite phase.

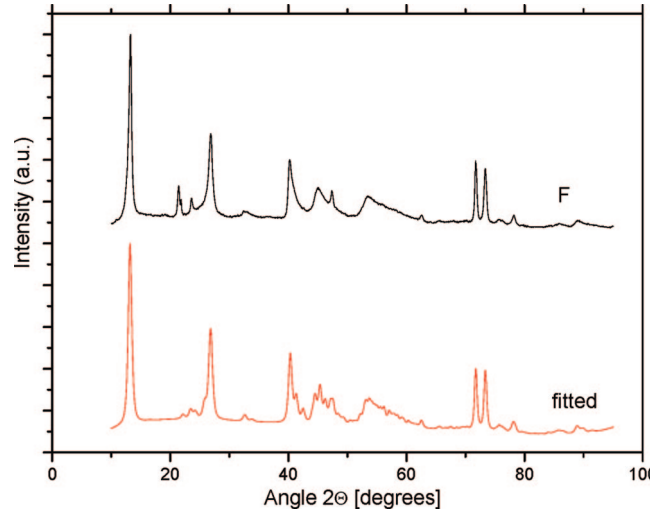

Figure 5. X-ray powder diffractogram of system F (Table 1) and the fitted diffractogram.

size of the particles was measured with imaging software (iTEM, soft imaging system GmbH). The surface area (A) of well over 250 individual particles was measured. An equivalent spherical diameter was calculated as

$$d = \sqrt{\frac{4A}{\pi}} \tag{1}$$

where A is the measured surface area. The polydispersity in the calculated diameters is expressed by means of the relative standard deviation

$$\sigma_d = \frac{\sqrt{\langle d^2 \rangle - \langle d \rangle^2}}{\langle d \rangle} \tag{2}$$

AFM measurements were performed using a scanning probe microscope (Digital Instruments) in tapping mode equipped with a TESP silicon tip (Digital Instruments) on a hydrotalcite suspension dried on freshly cleaved mica. In addition to the diameter, the thickness and its relative standard deviation (σ_l) of the platelets was measured from AFM images using WSxM (Nanotec electronica S.L.).

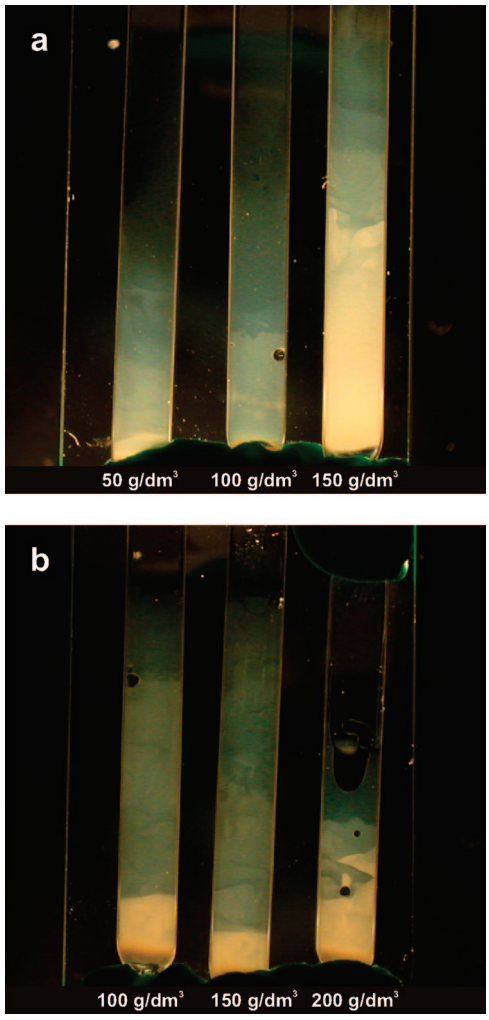

Figure 6. Sedimentation profiles of aqueous hydrotalcite between crossed polarizers at (a) 10^{-3} M NaCl added and from left to right 50, 100, and 150 g/dm^3 hydrotalcite and (b) 10^{-4} M NaCl added salt and from left to right 100, 150, and 200 g/dm^3 hydrotalcite.

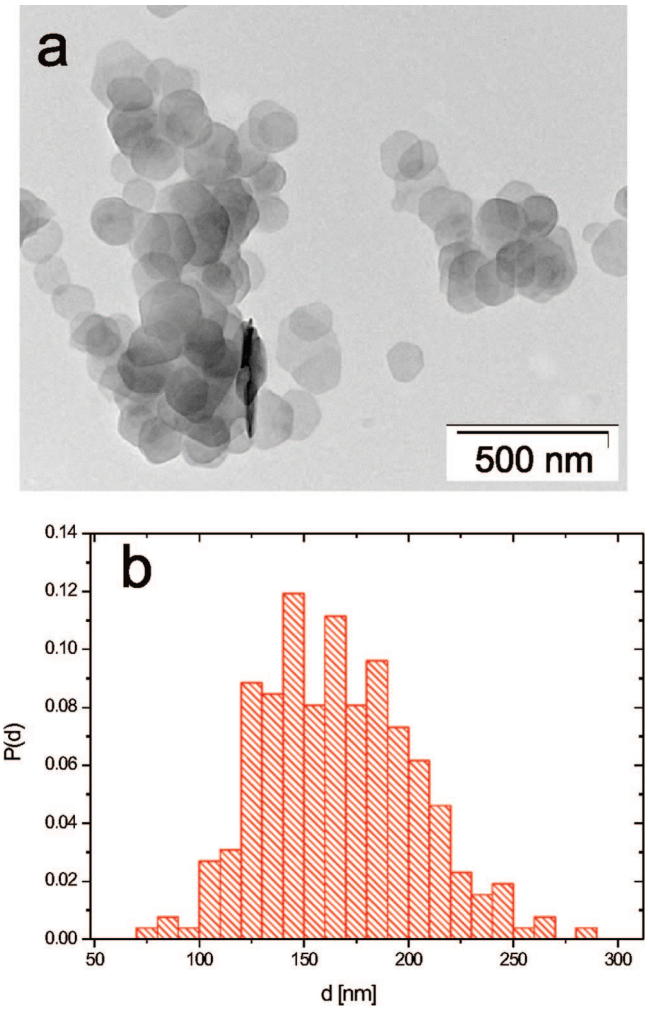

Figure 7. (a) Transmission electron micrograph of PIB grafted hydrotalcite platelets. The particle diameter was obtained from similar micrographs of the polymer grafted system yielding $\langle d \rangle = 167$nm and $\sigma = 0.22$ for the mineral core visible by TEM. Panel (b) shows a histogram of the average particle diameter distribution for the polymer grafted system as obtained by measurements on several electron micrographs as described in section 2.2.

Further characterization of the platelets was done by X-ray diffraction (XRD) using Co Kα radiation (1.79026 Å) on a Bruker-AXS D8 instrument operated at 30 kV and 45 mA. The powder X-ray diffractograms were compared with a powder diffraction database (International Centre for Diffraction Data, 2000), and Pawley fits were made in order to calculate the crystallographic unit cell constants using Topas (Bruker AXS, Delft, The Netherlands).

2.3. Sedimentation. The hydrotalcite platelets that were most likely to form nematic phases due to their large average diameter and therefore large (d/l) even in combination with an electric double layer were concentrated by centrifugation and redispersion in NaCl solutions. It is well-known that changing the ionic strength influences the interaction potential of charged particles and disk shaped particles in particular.[33] Therefore, a concentration series of 50−200 g/dm^3 was made in solutions of 10^{-3} and 10^{-4} M NaCl. The series was transferred into capillaries (Vitrocom, 100 mm × 4 mm, optical path = 100 μm) that were flame sealed and stored in the vertical position for sedimentation over several months. All samples were stored in a dark, thermostatted room and inspected regularly under normal illumination and between crossed polarizers.

Samples of PIB-stabilized hydrotalcite were prepared by centrifugation and redispersion in toluene in optical cells (10 × 10 × 40 mm^3, Hellma). These were inspected under normal illumination and between crossed polarizers during the first days after preparation and were stored upright for sedimentation during several months. A part of each sample was transferred to round borosilicate Mark tubes (diameter = 2 mm, W. Muller, Schonwalde bei Berlin, Germany) suitable for small-angle X-ray scattering experiments. Another part of each sample was transferred into homemade glass cuvettes of inner dimensions 10 × 10 mm^2 and approximately 145 μm for polarization microscopy.

Polarization Microscopy. A Nikon polarization microscope (Eclipse LV100pol) equipped with a digital camera (QImaging, MP5) was used to follow the phase separation process. A retardation filter (optical path difference = 530 nm) was inserted at an angle of 45° with respect to the polarizer and analyzer in order to determine the optical birefringence. Photographs were taken during the process of phase separation starting 2 h after homogenization.

3. Aqueous Dispersions

3.1. Temperature Controlled Synthesis of Nanoplatelets. After alkaline coprecipitation, crystalline platelets of hydrotalcite were hydrothermally treated. The effect of temperature

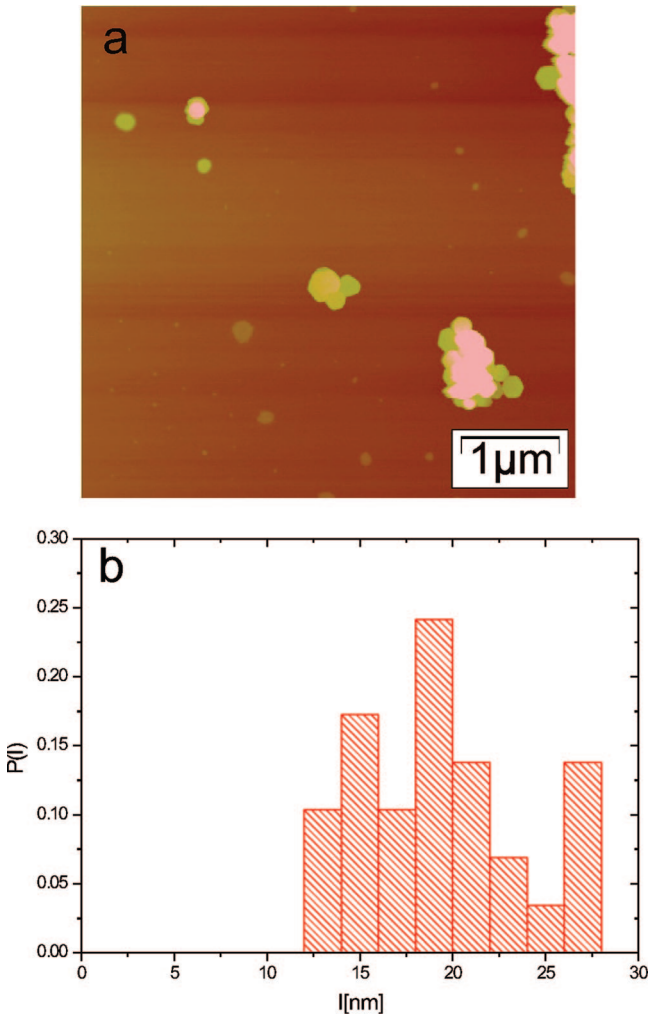

Figure 8. AFM measurements on polymer grafted hydrotalcite platelets. In panel (a), an AFM image of the polyisobutylene stabilized hydrotalcite platelets on a mica support is displayed. In panel (b), a histogram of the thickness of the grafted platelets, as measured by AFM, is shown ($\langle l \rangle = 19.2$ nm with $\sigma_l = 0.22$).

and salinity during this hydrothermal treatment and the ratio of Mg and Al ions on the size of the particles was determined by measurements of the average particle diameter. Figure 1 shows typical transmission electron micrographs of the systems obtained with hydrothermal treatment at different temperatures. The platelets have a hexagonal shape with rounded corners. There are no signs of aggregation visible in the micrographs.

Size distributions (as shown in Figure 2) were constructed from measurements on well over 250 particles, and the average diameter and the relative standard deviation were obtained (Table 1). The average diameter $\langle d \rangle$ ranges from 49 to 146 nm, and it became larger when hydrothermal treatment was performed at 150 instead of 85 °C as has been reported earlier.[21]

System C which has the largest particles and the lowest polydispersity in diameter was selected for further study. As a first step, we determined the thickness (l) and diameter (d) of the particles of this system by AFM. Images and histograms of (l) and (d) based on 100 particles are given in Figure 3. Using these results, we find an average thickness $\langle l \rangle = 12.7$ nm with a relative standard deviation $\sigma_l = 0.36$ and an average diameter $\langle d \rangle = 182$ nm with relative standard deviation $\sigma_d = 0.23$. The average diameter is larger than the value found by TEM. This may be related to the sampling. These AFM data allow us to investigate to what extent the diameter and thickness are correlated. The correlation coefficient

$$R_{d,l} = \frac{\langle dl \rangle - \langle d \rangle \langle l \rangle}{\langle d \rangle \langle l \rangle} \tag{3}$$

turns out to be 0.04. The product was identified to be hydrotalcite from the obtained powder X-ray diffraction patterns. One of the samples (F) shows signs of a bayerite phase in addition to hydrotalcite. Samples D and E have some minor unidentified peaks (see Figure 4). The sample that was hydrothermally treated without replacement of the mother liquid (D) appears less crystalline in comparison to sample E as individual widths of reflections are increased. The patterns were fitted to the *R*3*m* space group using the Pawley fit algorithm to yield a, b, and c parameters for the crystallographic unit cell (shown in Table 2, the X-ray powder diffractogram of system F and the corresponding fitted diffractogram are provided.

3.2. Sedimentation. By centrifugation and redispersion, hydrotalcite samples of system C were prepared at concentrations from 50 to 200 g/dm^3 and at ionic strengths ranging from 10^{-4} to 10^{-3} M NaCl in flat optical capillaries. The colloidal suspensions are stable both with and without the NaCl added and do not show any signs of aggregation. The sample at 200 g/dm^3 and 10^{-3} M NaCl was too viscous to be transferred into an optical capillary. Gravity induces sedimentation of the stable suspensions within days. After a few weeks, a remarkably complex pattern of layers is formed within the sediment. The layers are not separated by flat and horizontal interfaces, although distinct transitions between regions with a large variation in turbidity can be discerned. These patterns bear some resemblance to those described by Fossum et al. for sodium fluorohectorite.[34,35] Moreover, the sedimented samples are highly viscous and have deformed suspension−air interfaces. Figure 6 shows the samples 10 months after preparation between crossed polarizers. No birefringent phases were observed, although in some of the samples a birefringent speckle pattern typically sized 3−10 μm was observed. Therefore, a macroscopic nematic phase does not appear to have been formed.

4. Organic Dispersions

4.1. Synthesis of Organophilic Nanoplatelets. Freeze-drying a mixture of the aqueous system C with stabilizing SAP 230 TP polymer in 1-propanol yielded a sticky paste which easily dissolved in toluene. In three cycles of centrifugation and redispersion in toluene, the excess of polymer is removed and a stable, transparent dispersion of hydrotalcite in toluene remains. Dilute suspensions are colored yellow by optical absorption due to the SAP 230 TP and show birefringence upon stirring. As the index of refraction of hydrotalcites is close to that of toluene (≈1.50), the dispersion has a very low turbidity. Transmission electron micrographs (Figure 7a) were analyzed to determine the dimensions of the particles. The average diameter of the polymer grafted hydrotalcite particles is represented by the histogram in Figure 7b. The organophilic system has a larger average diameter and smaller polydispersity ($\langle d \rangle = 167$, $\sigma_d = 0.22$) compared to those of the original aqueous system, probably due to the size selective character of repetitive centrifugation and decantation. In Figure 8, we present an AFM image of the organophilic hydrotalcite platelets. Compared to the case of the aqueous system, presented in Figure 3, the spreading of the organophilic particles on mica

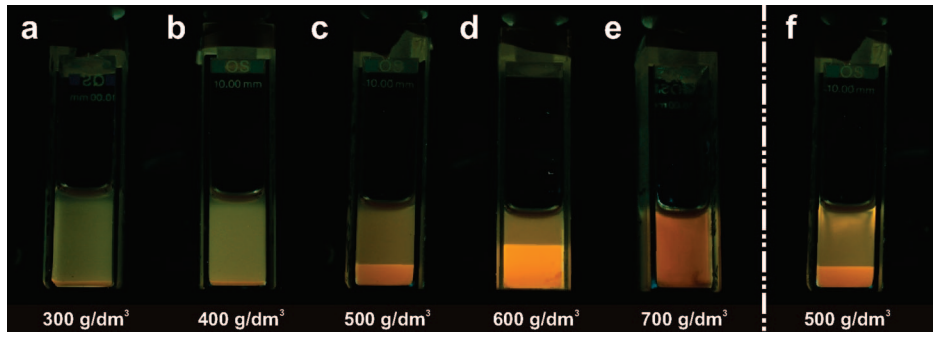

Figure 9. Isotropic−nematic phase separation of polyisobutylene stabilized hydrotalcite platelets in toluene as observed between crossed polarizers 2 days after homogenization. At concentrations of (a) 300 and (b) 400 g/dm^3, mainly the isotropic phase is visible. At (c) 500 and (d) 600 g/dm^3, a nematic phase appears clearly at the bottom of the cuvette which extends over the entire cuvette at (e) 700 g/dm^3. The lower phase is permanent birefringent; the upper phase shows birefringence when flow is induced by gently displacing the cuvette over millimeters, which is shown for (f) 500 g/dm^3.

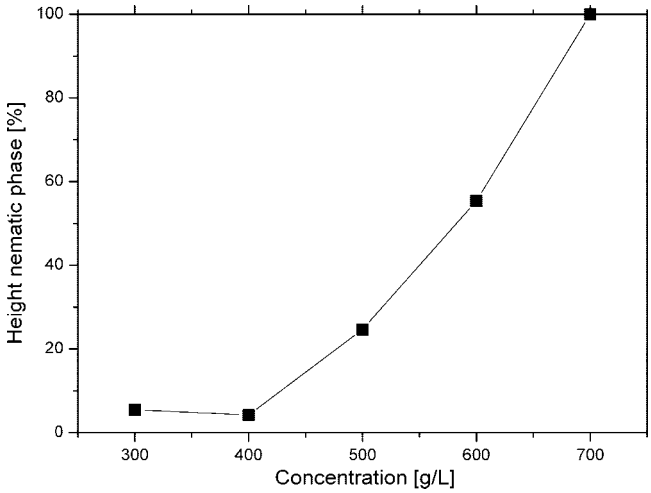

Figure 10. Phase volume of the nematic phase as part of the total volume for the samples shown in Figure 9. Three days after homogenization, the height of the nematic phase as part of the total volume in the capillaries was measured.

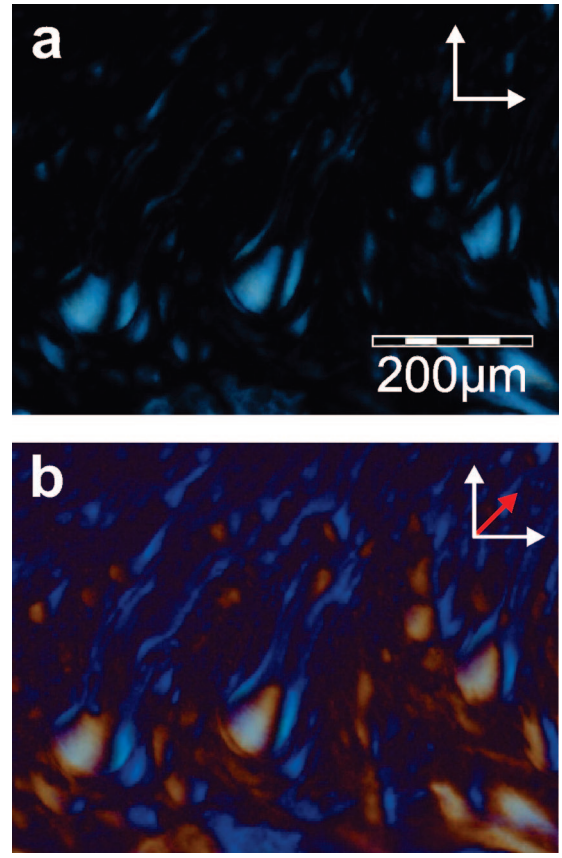

Figure 11. (a) Polarized light image of nematic tactoids in the isotropic phase showing tactoids ranging in size from approximately 20 to 75 μm in diameter between crossed polarizers. In panel (b), the same tactoids are depicted after insertion of a retardation filter of optical path difference 530 nm (slow axes indicated).

is rather poor, leading to overlaps. This makes determination of the diameter difficult, while the thickness could be sampled at the free edges of particles. The measurements reveal an average thickness $\langle l \rangle = 19.2$nm with a relative standard deviation $\sigma_l = 0.22$. Compared to the bare hydrotalcite particles, the SAP 230 TP covered hydrotalcite particles are on average 6.5 nm thicker, which is in reasonable agreement with twice the estimated thickness (3−4 nm) of the polyisobutylene grafting layer.[39,30]

4.2. Isotropic−Nematic Phase Separation. A series of concentrated nonaqueous dispersions of hydrotalcite was prepared in order to study phase separation of the platelets. Within 1 day, macroscopic phase separation is visible, and the samples split into a lower birefringent and a upper nonbirefringent phase (Figure 9a−e). The latter phase shows flow induced birefringence when the cuvette is gently displaced (Figure 9f). The interface between the isotropic and nematic phase moves along when the cuvettes are tilted. After 3 days, the relative phase volumes were measured, and they are presented in Figure 10.

In order to compare with other systems, the experimental value at which dispersions were at high enough concentration to undergo the isotropic−nematic transition can be converted in a so-called dimensionless density ($n\langle d^3 \rangle$, where n represents the number density (N/V) and d is the diameter of the platelets). The experimental volume fraction for a polydisperse system, ϕ, can easily be converted to dimensionless number densities. The particles are assumed to have a disk shape with diameter d and thickness l, so the volume fraction can be described as

$$\varphi = \frac{\pi}{4} n \langle d^2 l \rangle \tag{4}$$

The dimensionless number density can now be written as follows:

$$n\langle d^3\rangle = \frac{4}{\pi}\varphi\frac{\langle d^3\rangle}{\langle d^2 l\rangle} \quad (5)$$

Starting from this equation, sample calculations based on the obtained AFM data show that the dimensionless number density is rather accurately given by

$$n\langle d^3\rangle \simeq \frac{4}{\pi}\varphi\frac{\langle d\rangle}{\langle l\rangle} \quad (6)$$

Combining the TEM and AFM measurements, we use $\langle d\rangle = 173.5$ nm and $\langle l\rangle = 19.2$ nm. The quoted value for $\langle d\rangle$ is based on the TEM value (167 nm) plus the thickness of the stabilizing polyisobutylene layers (6.5 nm) inferred from AFM measurements. The volume fraction ϕ is calculated as the solid mass content of the dispersion per volume divided by the particle density (ρ) of the composite hydrotalcite−polymer particle. The composite mass density was estimated at 1.70 kg/dm^3 by taking into account a 12.7 nm thick disk of mineral hydrotalcite with mass density 2.13 kg/dm^3 and a total thickness of 6.5 nm of the polyisobutylene stabilizing layers with density 0.87 kg/dm^3. The threshold concentration at which the biphasic region starts is estimated by extrapolation of the data in Figure 10 to be 0.400 kg/dm^3 (the origin of the small nematic phase observed after 3 days at an overall concentration of 300 g/dm^3 is ascribed to sedimentation). This mass density corresponds to a volume fraction $\phi_I = 0.24$ and hence $n_I\langle d^3\rangle = 2.75$. Similarly, a value of $\phi_N = 0.41$, and hence, $n_N\langle d^3\rangle = 4.70$ is found after insertion of the mass concentration at which samples are fully nematic (0.700 kg/dm^3). In Table 3). In Figure 5, this value is compared with experimental and computer simulation data for isotropic−nematic phase separating systems of platelets. Computer simulations for monodisperse systems give a relative width of the biphasic gap of about 10% or slightly less, whereas for a 25% polydisperse system the width of the biphasic gap is 40%. The experimental system studied here gives a width of the biphasic region of 75%. This is higher than the theoretical value for infinitely thin platelets and clearly indicates the importance of polydispersity in experimental systems.

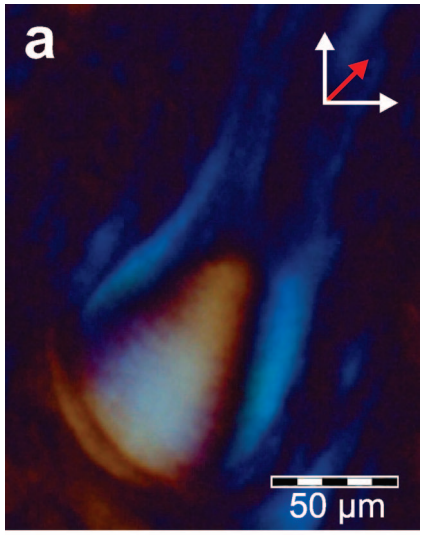

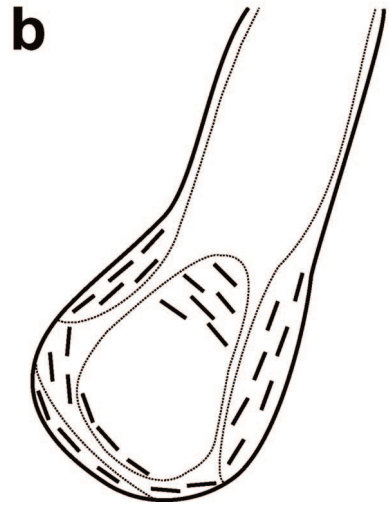

Figure 12. (a) Closeup of one of the tactoids presented in Figure 11b. (b) Artist impression of the orientation of the platelets within the intersect of the nematic tactoid represented in panel (a) as deduced from the interference colors in combination with the orientation of the retardation filter.

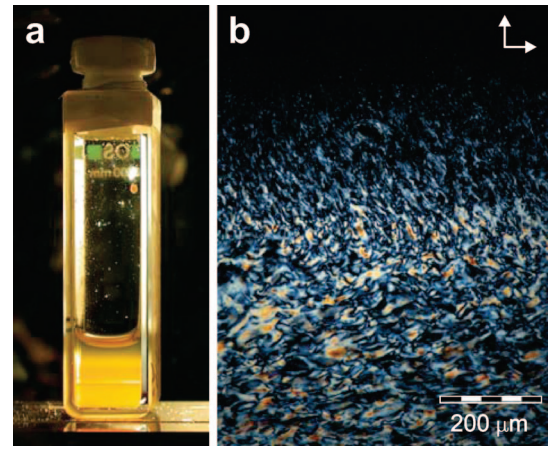

Figure 13. (a) Macroscopic and (b) microscopic observations of the isotropic−nematic interface at 500 g/dm^3 between crossed polarizers (indicated by the arrows), 4 months after homogenization. (a) On top of the initial interface, a 1 mm thick layer of birefringent material is visible. (b) The initially sharp interface is coarsened such that there is no longer a sharp interface between the nematic and the isotropic phase but a diffuse layer of tactoids instead.

TABLE 3: Comparison of $n\langle d^3\rangle$ for the Concentration of the Isotropic to Nematic Transition As Found in This Study and in Literature[a]

reference	experiment	(d/l)	$n_I\langle d^3\rangle$	$n_N\langle d^3\rangle$
this study	PIB grafted hydrotalcite	9	2.75	4.70
30	PIB grafted gibbsite	11	2.5	2.7
46	Monte Carlo	∞	4.04	4.12
47	Monte Carlo cut spheres	10	3.82	3.87
48	Monte Carlo cut spheres	10	4.03	4.17
42	Monte Carlo cut spheres	15	3.68	4.11
48	Monte Carlo cut spheres	20	3.90	4.17
49	Monte Carlo, 25% polydispersity	∞	3.53	4.97

[a] The value $n_I\langle d^3\rangle$ refers to the lower boundary of the biphasic gap, while $n_N\langle d^3\rangle$ refers to the higher boundary.

4.3. Nematic Tactoids. Nematic tactoids are observed to nucleate and sediment in the isotropic phase. Typically, they have dimensions ranging from 20 to 70 μm in diameter and are found to have a rather round shape that is elongated, giving rise to tails along the direction of sedimentation. This is exemplified in Figure 11 where a microscopy image of the isotropic phase close to the isotropic−nematic interface in a biphasic sample between crossed polarizers is shown. To identify the structure of the nematic tactoids, retardation plates were used.

Hydrotalcite is a uniaxial negative material ($n_\epsilon = 1.494$, $n_\omega = 1.511$,[40] and references included). This means that the slow

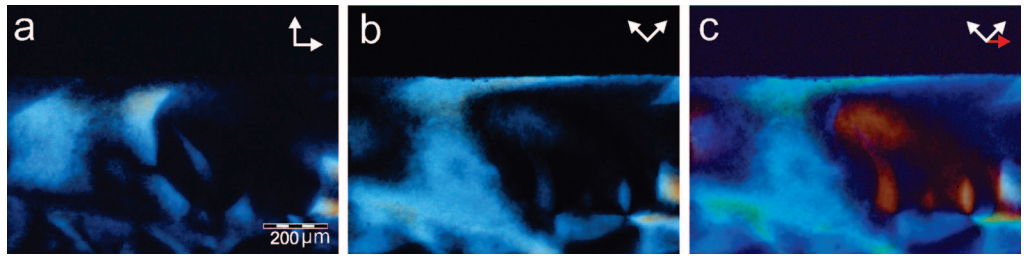

Figure 14. Polarization microscope images of the sedimentation induced isotropic−nematic interface of polymer grafted hydrotalcite. (a) The crossed polarizers are oriented parallel and perpendicular with respect to the interface. (b) Rotation of the polarizers by 45° results in a clear visibility of the interface and therefore indicates that the particles have a preferential orientation with respect to the interface. (c) Insertion of a retardation filter at 45° with respect to the polarizers reveals the orientation of the particles at the interface: higher interference colors blue and green are observed which are related to the slow axis of the particles being parallel to the interface.

axes are directed along the surface of the platelets. Since the difference in refractive indices of the solvent toluene ($n = 1.496$) and hydrotalcite ($n \simeq 1.5$) is very small, the birefringence of the nematic phase will be determined by the intrinsic birefringence of the mineral platelets themselves.[41] This means that in the nematic phase the slow axes are perpendicular to the director, which is defined as the vector perpendicular to the surface of the platelets. Therefore, polarization microscopy pictures taken with a retardation filter in the optical system will display higher interference colors if the director is oriented perpendicular to the slow axis of the retardation filter and the optical axis of the microscope. It should be noted that no contribution to birefringence and therefore no interference color comes from those particles with a director parallel to the microscope axis or parallel to one of the polarizers.

The orientation of the director at different locations within the nematic tactoids may now be determined. From the interference colors with and without a retardation filter, we deduce that the platelets align parallel to the interface of the tactoids in agreement with the observations done by van der Beek et al. on the orientation of sterically stabilized gibbsite platelets at the macroscopic isotropic−nematic interface.[42]

The blue interference color observed with a retardation filter on the left and right side of the tactoid corresponds to an optical path difference of 680 nm (Michel−Levy color chart). Subtracting the contribution of the retarder means that the optical path difference Γ is 150 nm. Since

$$\Gamma = \Delta n s \tag{7}$$

we find using a path length (s) of 50 μm a Δn value equal to 0.003. Comparing this to the estimated theoretical value,

$$\Delta n = |n_\epsilon - n_\omega| \phi_{\text{core}} S_2 \tag{8}$$

using for the volume fraction of hydrotalcite cores $\phi_{\text{core}} = 0.25$ and for the order parameter $S_2 \simeq 0.8$, we find $\Delta n = 0.0033$. This is in good agreement with the value that follows from polarization microscopy and confirms our analysis. In the lower part of the tactoid, we observe an orange-yellow interference color of 380 nm. This corresponds to an optical difference of 150 nm again but now in the subtraction mode. Combining the observation described above, a sketch of the particle orientation at the surface of the tactoid can be made (Figure 12). The interference color in the core of the tactoid, however, is more complex to analyze due to the cumulative character of the interference colors and is therefore not analyzed.

Interestingly, it seems that the nematic tactoids are reluctant to merge with the nematic phase upon arrival at the interface. In Figure 13, the sample at 500 g/dm^3 is presented, 4 months after preparation. On top of the initial interface, a new layer of birefringent material is deposited. If we observe this at a microscopic level, we find that there is an extended layer of tactoids present on top of the interface.

4.4. Sedimentation. Samples with overall concentrations of 275 and 350 g/dm^3 that initially are in the isotropic phase develop nematic phases due to sedimentation. The first signs of this sedimentation induced isotropic−nematic transition are observed already after a few days. The nematic phase just below the interface consists of many small nematic domains with a typical size in the order of 10 μm. In time, the nematic domains merge and the interface becomes more smooth and flat. Figure 14 shows polarization microscopy images of the sedimentation induced isotropic to nematic transition at 350 g/dm^3 after 4 months when full sedimentation equilibrium appears to have been reached.

When the crossed polarizers are oriented parallel and perpendicular with respect to the interface (Figure 14a), no birefringence at the interface is observed, indicating that the director of the platelets at the interface is directed along one one of the crossed polarizers. This is confirmed by the appearance of interference colors at the interface upon rotation of the polarizers by 45° (Figure 14b). Insertion of a 530 nm retardation filter at 45° with respect to the polarizers leads to the appearance of higher interference colors blue and green, indicating that the slow optical axis is parallel to the interface (Figure 14c). This in turn means that the particles are parallel to the interface as was observed for colloidal gibbsite.[43,42]

In the case of the sample at 275 g/dm^3, the volume fraction of the nematic phase is 0.208; in the case of 350 g/dm^3, this fraction is 0.283 in sample cells with a height of 12 mm. Assuming the concentration of the nematic phases to be equal to 700 g/dm^3, we find for the average concentration in the isotropic phase 163 g/dm^3 in the case of an overall concentration of 275 g/dm^3 and 212 g/dm^3 for an overall concentration of 350 g/dm^3. This means that there is a large difference in the overall concentrations of isotropic phases in equilibrium with a sedimentation induced nematic phase. Using the equations of state for osmotic pressure as obtained from Monte Carlo simulations, the concentration profiles in the various phases can be calculated.

For a monodisperse colloidal suspension, the balance between the osmotic pressure gradient and the gravitational force can be written as follows:

$$\frac{\partial \Pi}{\partial z} = -nm^* g \tag{9}$$

where Π is the osmotic pressure, z is the height of the phase, n is the particle number density (number of particles per volume, N/V), m^* is the buoyancy corrected mass of the colloidal hydrotalcite particles, and g is the gravitational force constant. Equation 9 can be rewritten in the form

$$\left(\frac{\partial \Pi}{\partial n}\right)_{T,\mu_0} \frac{\partial n}{\partial z} = -nm^* g \tag{10}$$

where T refers to the absolute temperature and μ_0 refers to the chemical potential of the solvent. For the case of sterically stabilized gibbsite, the heights of the phases were calculated and reasonable agreement with experiments was obtained.[42]

For the present system, polydispersity plays a significant role as is exemplified from the width of the biphasic gap. In order to take the effect of polydispersity into account, one has to define a balance equation of the different species:[44]

$$\frac{\partial \mu_j}{\partial z} = -m_j^* g \qquad j = 1, \ldots, c \tag{11}$$

which in turn can be written as

$$\sum_{k=1}^{c} \left(\frac{\partial \mu_j}{\partial n_k}\right)_{T,\mu_0,n_l} \frac{\partial n_k}{\partial z} = -m_j^* g \qquad j = 1, \ldots, c \tag{12}$$

Although for binary mixtures of hard spheres good expressions for the thermodynamic derivatives

$$\left(\frac{\partial \mu_j}{\partial n_k}\right)_{T,\mu_0,n_l} \tag{13}$$

exist and therefore concentration profiles could be calculated,[45] the required thermodynamic derivatives for platelets are not known and similar calculations could not been performed.

5. Conclusions

In this work, double layered hydroxides were synthesized from magnesium and aluminum nitrates controlling the size of the platelets to tailor them to platelet sizes applicable for lyotropic liquid crystal formation by adjustment of the reactants and the temperature of hydrothermal treatment. The aqueous colloidal suspensions are highly stable, and on prolonged standing (10 months) interesting sedimentation profiles are formed, but no liquid crystal transitions were observed. Liu et al.[16] reported on similar sedimentation profiles in which nematic phases are formed after several weeks as evidenced by clear birefringence and tactoid formation. It should be noted that the concentrations of the suspensions that formed nematic phases were very close to the sol−gel transition.[36] Apparently, in our system, like in most natural and synthetic aqueous clay systems, the sol−gel transition occurs before the isotropic−nematic phase separation.[37,38] Using a novel approach involving freeze-drying, amino-functionalized polyisobutylene was grafted on the inorganic platelets. This stabilizer proved its use in other liquid crystal forming systems.[9,18,19] The organophilic disks prepared here also showed isotropic−nematic phase transitions at very short time scales. This transition occurs at a concentration similar to comparable systems found in the literature, although the biphasic gap is wider than that observed so far. Moreover, nematic tactoids are observed in polarization microscopy. Nematic phases were induced by gravity in initially isotropic samples, yielding sharp isotropic−nematic interfaces. As has been argued in ref 19, the grafting with PIB leads to (nearly) hard particle interactions, which makes the suspension less susceptible to gelation, allowing for the isotropic−nematic phase transition to be observed.

Acknowledgment. The authors thank M. Versluijs-Helder for performing the X-ray diffraction and analysis, and J. W. ten Brinke is thanked for exploratory synthesis experiments. H. Meeldijk and the Electron Microscopy Group (Utrecht University) are thanked for assistance with TEM. The Dutch Organisation for Scientific Research (NWO) is thanked for financial support of M.C.D.M., and Schlumberger Limited Company is acknowledged for financial support of M.M.v.S. Infineum (U.K.) is acknowledged for donation of the SAP 230TP.

References and Notes

(1) Sonin, A. S. *J. Mater. Chem.* **1998**, *8*, 2557.
(2) Davidson, P.; Gabriel, J.-C. P. *Curr. Opin. Colloid Interface Sci.* **2005**, *9*, 377.
(3) Zocher, H. *Z. Anorg. Allg. Chem.* **1925**, *147*, 91.
(4) Coper, K.; Freundlich, H. *Trans. Faraday Soc.* **1937**, *33*, 348.
(5) Langmuir, I. *J. Chem. Phys.* **1938**, *6*, 873.
(6) Bihannic, I.; Michot, L. J.; Lartriges, B. S.; Vantelon, D.; Labille, J.; Thomas, F.; Susini, J.; Salomé, M.; Fayard, B. *Langmuir* **2001**, *17*, 4144.
(7) Onsager, L. *Ann. N. Y. Acad. Sci.* **1949**, *51*, 627.
(8) Bugosh, J. *J. Phys. Chem.* **1961**, *65*, 1789.
(9) Buining, P. A.; Philipse, A. P.; Lekkerkerker, H. N. W. *Langmuir* **1994**, *10*, 2106.
(10) Kajiwara, K.; Donkai, N.; Hiragi, Y.; Inagaki, H. *Makromol. Chem.* **1986**, *187*, 2883.
(11) Maeda, Y.; Hachisu, S. *Colloids Surf.* **1983**, *6*, 1.
(12) Maeda, H.; Maeda, Y. *Phys. Rev. Lett.* **2003**, *90*, 018303.
(13) Lemaire, B. J.; Davidson, P.; Petermann, D.; Panine, P.; Dozov, I.; Stoenescu, D.; Jolivet, J. P. *Eur. Phys. J. E* **2004**, *13*, 309.
(14) Lemaire, B. J.; Davidson, P.; Ferré, J.; Jamet, J. P.; Panine, P.; Dozov, I.; Jolivet, J. P. *Phys. Rev. Lett.* **2002**, *88*, 125507.
(15) van der Beek, D.; Lekkerkerker, H. N. W. *Europhys. Lett.* **2003**, *61*, 702.
(16) Liu, S.; Zhang, J.; Wang, N.; Liu, W.; Zhang, C.; Sun, D. *Chem. Mater.* **2003**, *15*, 3240.
(17) Michot, L. J.; Bihannic, I.; Maddi, S.; Funari, S. S.; Baravian, C.; Levitz, P.; Davidson, P. *Proc. Natl. Acad. Sci. U.S.A.* **2006**, *103*, 16101.
(18) van der Kooij, F. M.; Kassapidou, K.; Lekkerkerker, H. N. W. *Nature* **2000**, *406*, 868.
(19) Zhang, Z. X.; van Duijneveldt, J. S. *J. Chem. Phys.* **2006**, *124*, 154910.
(20) Vaccari, A. *Catal. Today* **1998**, *41*, 53.
(21) Hickey, L.; Kloprogge, J. T.; Frost, R. L. *J. Mater. Sci.* **2000**, *35*, 4347.
(22) Lagaly, G.; Mecking, O.; Penner, D. *Colloid Polym. Sci.* **2001**, *279*, 1090.
(23) Wang, N.; Liu, S.; Zhang, J.; Wu, Z.; Chen, J.; Sun, D. *Soft Matter* **2005**, *1*, 428.
(24) Zhu, W.; Sun, D.; Liu, S.; Wang, N.; Zhang, J.; Luan, L. *Colloids Surf., A* **2007**, *301*, 106.
(25) Wijnhoven, J. E. G. J.; van 't Zand, D. D.; van der Beek, D.; Lekkerkerker, H. N. W. *Langmuir* **2005**, *21*, 10422.
(26) Mourad, M. C. D.; Wijnhoven, J. E. G. J.; Van 'T Zand, D. D.; van der Beek, D.; Lekkerkerker, H. N. W. *Philos. Trans. R. Soc. London, Ser. A* **2006**, *364*, 2807.
(27) Veerman, J. A.C.; Frenkel, D. *Phys. Rev. A* **1990**, *41*, 3237.
(28) Brown, A. B. D.; Clarke, S. M.; Rennie, A. R. *Langmuir* **1998**, *14*, 3129.
(29) Buining, P. A.; Lekkerkerker, H. N. W. *J. Phys. Chem.* **1993**, *97*, 11510.
(30) van der Kooij, F. M.; Lekkerkerker, H. N. W. *J. Phys. Chem. B* **1998**, *102*, 7829.
(31) Heux, L.; Chauve, G.; Bonini, C. *Langmuir* **2000**, *16*, 8210.
(32) Fu, X.; Qutubuddin, S. *Polymer* **2001**, *42*, 807.
(33) Verwey, E. J. W.; Overbeek, J. T. G. *Theory of the Stability of Lyophobic Colloids*; Elsevier: Amsterdam, 1948.
(34) Fossum, J. O. *Physica A (Amsterdam)* **1999**, *270*, 270.
(35) Fossum, J. O.; Gudding, E.; Fonseca, D. d. M.; Meheust, Y.; DiMasi, E.; Gog, T.; Venkataraman, C. *Energy* **2005**, *30*, 873.
(36) Zhang, J.; Luan, L. Y.; Zhu, W. X.; Liu, S. Y.; Sun, D. J. *Langmuir* **2007**, *23*, 5331.
(37) Mourchid, A.; Delville, A.; Lambard, J.; Lécolier, E.; Levitz, P. *Langmuir* **1995**, *11*, 1942.
(38) Gabriel, J. C. P.; Sanchez, C.; Davidson, P. *J. Phys. Chem.* **1996**, *100*, 11139.
(39) van Bruggen, M. P. B.; van der Kooij, F. M.; Lekkerkerker, H. N. W. *J. Phys.: Condens. Matter* **1996**, *8*, 9451.
(40) Frondel, C. *Am. Mineral.* **1941**, *26*, 295.
(41) Bragg, W. L.; Pippard, A. B. *Acta Crystallogr.* **1953**, *6*, 865.
(42) van der Beek, D.; Schilling, T.; Lekkerkerker, H. N. W. *J. Chem. Phys.* **2004**, *121*, 5423.

(43) van der Beek, D.; Lekkerkerker, H. N. W. *Langmuir* **2004**, *20*, 8582.
(44) Vrij, A. *J. Chem. Phys.* **1980**, *72*, 3735.
(45) Biben, T.; Hansen, J. P.; Barrat, J. L. *J. Chem. Phys.* **1993**, *98*, 7330.
(46) Eppenga, R.; Frenkel, D. *Mol. Phys.* **1984**, *52*, 1303.
(47) Veerman, J. A. C.; Frenkel, D. *Phys. Rev. A* **1992**, *45*, 5632.
(48) Zhang, S.-D.; Reynolds, P. A.; van Duijneveldt, J. S. *J. Chem. Phys.* **2002**, *117*, 9947.
(49) Bates, M. A. *J. Chem. Phys.* **1999**, *111*, 1732.

JP803114V